

Reports

Observations of Strain Accumulation Across the San Andreas Fault Near Palmdale, California, with a Two-Color Geodimeter

Abstract. *Two-color laser ranging measurements during a 15-month period over a geodetic network spanning the San Andreas fault near Palmdale, California, indicate that the crust expands and contracts aseismically in episodes as short as 2 weeks. Shear strain parallel to the fault has accumulated monotonically since November 1980, but at a variable rate. Improvements in measurement precision and temporal resolution over those of previous geodetic studies near Palmdale have resulted in the definition of a time history of crustal deformation that is much more complex than formerly realized.*

Studies of crustal deformation near Palmdale, California, reveal enigmatic patterns of strain accumulation and uplift. Particularly well known is the Palmdale bulge (1), in which the town of Palmdale reportedly rose 18 cm relative to Saugus, about 42 km to the southwest, between May and October 1961 (2). Almost as spectacular and unexpected was the discovery that during a 7-month period beginning in February 1979 the Palmdale trilateration network, straddling the San Andreas fault (Fig. 1A), underwent an areal expansion, or dilatation, of nearly 2 ppm (3).

These examples of anomalous aseismic deformation are as controversial as they are remarkable. Geophysicists are debating the details, and perhaps the reality, of both the Palmdale bulge (4) and the areal expansion (5). Although the anomalous crustal deformation has occurred without notable seismicity, these episodes are important because they might somehow foreshadow a repeat of the 1857 earthquake of magnitude 8 $\frac{1}{4}$ (6): the 400-km zone of rupture for this earthquake included most of the portion

of the San Andreas fault shown in Fig. 1A (7). Thus it is imperative to obtain new and more detailed information about patterns of strain accumulation in the Palmdale area. Accordingly, late in 1980 we began to measure distances with a two-color Geodimeter (8) to determine the crustal deformation near Pearblossom, California (Fig. 1A). In this report we describe our results and compare our new findings with those based on less frequent trilateration measurements made with a single-color laser Geodimeter during the last 10 years within the Palmdale network (9), about 40 km northwest of Pearblossom (see Fig. 1A).

Our Pearblossom network has 13 monuments radially distributed at distances between 3 and 8 km from the observatory, which is situated on a ridge several kilometers northeast of the San Andreas fault. Typically, the network has been surveyed twice a week, except during 3 weeks in October 1981 when the two-color Geodimeter was broken down.

A total of 1583 baseline measurements were made between 1 November 1980 (1980.83) and 6 February 1982 (1982.10).

We analyzed these data under the assumption of uniform strain throughout the network (Fig. 1B). Under this assumption, we determined the three independent components of the strain tensor as a function of time (t) in a coordinate system aligned with the local strike of the San Andreas fault, N65°W. These components are ϵ_{pp} and ϵ_{nn} , parallel and normal to the fault strike, respectively, and ϵ_{np} , the tensor shear strain corresponding to a right-lateral sense of displacement across the fault. Also shown in Fig. 1 is the dilatation, or areal expansion of the network, which is the sum $\epsilon_{pp} + \epsilon_{nn}$.

We also considered the possibility that strain did not accumulate homogeneously in the network. If the strain change is inhomogeneous within the Pearblossom network, then one would expect data from different subnetworks to yield significantly discordant results. The San Andreas fault defines an obvious division into two subnetworks for which disparate results might seem likely: Pearblossom northeast, consisting of the five lines to the northeast of the fault in Fig. 1B, and Pearblossom southwest, consisting of the eight fault-crossing lines in Fig. 1B. Table 1 shows the secular strain rates ($\dot{\epsilon}$) that best fit the data for the Pearblossom network and the subnetworks. None of the components for either of the subnetworks differs appreciably from those for the entire network. Accordingly, we retain our assumption of homogeneous strain accumulation (11) throughout the network.

The components of the strain tensor change differently in time (Fig. 1C). The tensor shear component ϵ_{np} generally increases at an average rate (Table 1) of about 0.16 ppm/year. However, from the first to the second half of the 15-month period of observations, the average rate for ϵ_{np} increases from 0.06 to 0.25 ppm/year (Table 1 and Fig. 1C). Thus, although ϵ_{np} accumulates monotonically, its rate appears to vary with time.

The normal component of strain ϵ_{nn}

Table 1. Strain rates in the Pearblossom and Palmdale networks.

Network	Interval	Tensor strain rates (ppm/year)			Principal strain rates (ppm/year)		Azimuth of $\dot{\epsilon}_1$
		$\dot{\epsilon}_{nn}$	$\dot{\epsilon}_{pp}$	$\dot{\epsilon}_{np}$	$\dot{\epsilon}_1$	$\dot{\epsilon}_2$	
Pearblossom	1980.83–1982.10	-0.01 ± 0.02	-0.10 ± 0.01	0.16 ± 0.01	0.12 ± 0.02	-0.22 ± 0.02	N62.2°E ± 1.8°
Pearblossom northeast	1980.83–1982.10	0.06 ± 0.02	-0.10 ± 0.02	0.13 ± 0.02	0.14 ± 0.03	-0.18 ± 0.03	N54.0°E ± 2.9°
Pearblossom southwest	1980.83–1982.10	-0.03 ± 0.02	-0.10 ± 0.02	0.18 ± 0.02	0.12 ± 0.03	-0.25 ± 0.02	N65.1°E ± 2.7°
Pearblossom	1980.83–1981.46	-0.09 ± 0.04	-0.26 ± 0.03	0.06 ± 0.03	-0.07 ± 0.04	-0.27 ± 0.04	N42.3°E ± 7.0°
Pearblossom	1981.46–1982.10	0.06 ± 0.04	0.04 ± 0.03	0.25 ± 0.03	0.30 ± 0.04	-0.20 ± 0.04	N69.4°E ± 3.2°
Palmdale	1971.6–1980.9	-0.05 ± 0.02	0.06 ± 0.02	0.18 ± 0.02	0.18 ± 0.02	-0.19 ± 0.02	N73.8°E ± 2.0°

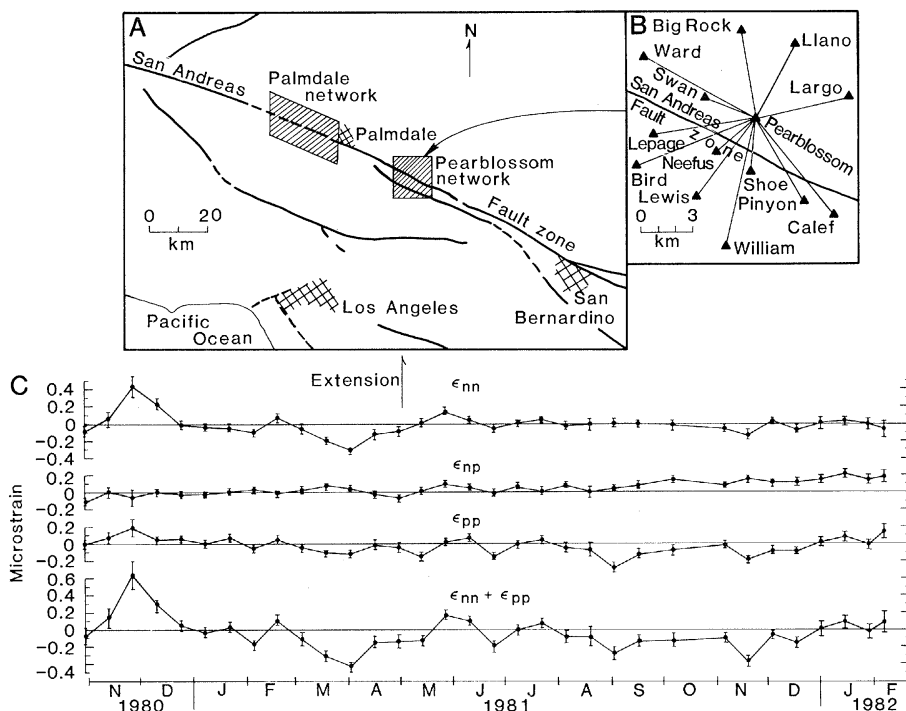


Fig. 1. (A) Map showing key tectonic features near Palmdale, California. (B) Pearblossom network. (C) Components of the strain tensor as a function of time plotted generally at 2-week intervals. Also shown is the dilatation, $\epsilon_{nn} + \epsilon_{pp}$.

has a secular rate (Table 1) that is nearly zero, but this component shows large departures from its secular trend (Fig. 1C). Notable episodes are an extension of ~ 0.5 ppm normal to the fault in November 1980, followed by nearly as much contraction during December, and a contraction of ~ 0.4 ppm from mid-February to April 1981, followed by about the same amount of extension over the next 2 months. During the latter half of the observational period ϵ_{nn} has shown only minor fluctuations.

The parallel strain component ϵ_{pp} exhibits smaller short-term fluctuations than ϵ_{nn} (Fig. 1C) but has a substantial secular rate. The secular rate is time-dependent; it is high and contractional during the first half of the observation period and low and extensional during the second half (Table 1). Some of the deviations of ϵ_{pp} from its secular trend are in phase with those of ϵ_{nn} and others occur when there is no noticeable fluctuation in ϵ_{nn} . For example, both components increased during November 1980, resulting in a marked episode of dilatation; but the largest fluctuation of ϵ_{pp} , from mid-August to mid-September 1981, was not accompanied by a detectable change in ϵ_{nn} .

The sum $\epsilon_{nn} + \epsilon_{pp}$, or the areal dilatation (Fig. 1C), indicates short-term fluctuations at peak rates as high as about 8 ppm/year for periods of a month and a secular decrease at an average rate of

0.10 ppm/year (12). However, the average rate is time-dependent; for example, had the observational period ended 1 month earlier, the secular rate of decrease would have been 0.22 ppm/year (13).

Our results and the results from the Palmdale network (9) have several features in common. (i) In both studies ϵ_{np} was found to accumulate monotonically, and the secular rate of this component for the Palmdale network from 1971 to 1980 is essentially the same as that found for the Pearblossom array (Table 1). (ii) Since the remarkable expansion of the Palmdale network in 1979, there have been several episodes of expansion and contraction (3, 9) with strain amplitudes comparable to those observed in the Pearblossom network during November 1980 and March and April 1981 (Fig. 1C). (iii) The secular principal strain rates and directions determined for the Pearblossom network are similar to those for Palmdale during the period from 1971 to late 1980. Thus the strain observations at Pearblossom are similar in most essential aspects to those made over the Palmdale network.

Because our measurements were made more frequently and with higher precision than those in previous studies, our results indicate that the strain in the vicinity of Pearblossom has more variability than was formerly thought. It remains to be seen whether these im-

provements in resolving strain accumulation will help to answer some of the essential questions regarding the mechanics of anomalous strain episodes and their possible relation to future great earthquakes.

J. O. LANGBEIN
M. F. LINKER
A. MCGARR

U.S. Geological Survey,
Menlo Park, California 94025

L. E. SLATER
Cooperative Institute for Research in
Environmental Sciences,
University of Colorado, Boulder 80309

References and Notes

1. R. O. Castle, J. P. Church, M.R. Elliott, *Science* **192**, 251 (1976).
2. R. K. Mark, J. C. Tinsley III, E. B. Newman, T. D. Gilmore, R. O. Castle, *J. Geophys. Res.* **86**, 2783 (1981).
3. J. C. Savage, W. H. Prescott, M. Lisowski, N. E. King, *ibid.* **86**, 6991 (1981).
4. W. E. Strange, *ibid.*, p. 2809.
5. A. Cheng and D. D. Jackson, *Eos* **63**, 430 (1982); R. C. Jachens, W. Thatcher, C. W. Roberts, R. S. Stein, *Science*, in press.
6. W. Thatcher, *Nature (London)* **299**, 12 (1982).
7. K. E. Sieh, *J. Geophys. Res.* **83**, 3907 (1978).
8. The two-color Geodimeter is owned by the University of Colorado at Boulder and had been operating in Hollister, Calif., from September 1975 until October 1980, when it was moved to the new observatory at Pearblossom [L. E. Slater and G. R. Huggett, *J. Geophys. Res.* **81**, 6299 (1976); G. R. Huggett, L. E. Slater, J. Langbein, *ibid.* **82**, 3261 (1977)]. By ranging with two lasers in different colors, red and blue, first-order corrections for variations in the speed of light due to changes in air density along the path can be made, yielding a baseline measurement that is precise to about 0.1 ppm. Because the distance measurements obtained from the two-color Geodimeter are relatively insensitive to the density of the atmosphere when compared to measurements from a single-color Geodimeter, we can make an end-point measurement of temperature, atmospheric pressure, and water vapor pressure to obtain a precision of 0.1 ppm in the distance measurement.
9. J. C. Savage, W. H. Prescott, M. Lisowski, N. E. King, *Science* **211**, 56 (1981).
10. The observed i th distance on the j th baseline, d_{ij} , is related to the strain tensor by

$$d_{ij} = \bar{D}_j + D_j [\epsilon_{pp}(t) \cos^2 \theta_j + 2\epsilon_{pn}(t) \sin \theta_j \cos \theta_j + \epsilon_{nn}(t) \sin^2 \theta_j]$$
 where \bar{D}_j , D_j , and θ_j are the adjusted line length, approximate line length, and azimuth of the j th baseline, respectively, and $\epsilon_{pp}(t)$, $\epsilon_{pn}(t)$, and $\epsilon_{nn}(t)$ are estimated values of strain at time t . The functional form of strain is arbitrary; for the analysis in Fig. 1, we used a function of segmented lines that have 2-week intervals. For the secular trends (Table 1), the line segments are either 7¹/₂ or 15 months in length. A least-squares procedure is used to determine \bar{D}_j and the parameters of the strain function. The absolute values of the strain and \bar{D}_j cannot be determined since the time of zero strain is arbitrary; thus the absolute values of the scales in Fig. 1 are arbitrary, but values of the strain changes are exact, if one assumes uniform strain accumulation.
11. However, the rate of accumulation of dextral shear strain appears to be almost 40 percent higher for the fault-crossing subnetwork than for the subnetwork to the northeast. If more data confirm this contrast in ϵ_{np} , it will be necessary to consider the possibility of enhanced shear strain accumulation in the San Andreas fault zone, which might be due to reduced elastic moduli or strength relative to the surrounding rock.
12. If the line length measurements were affected by a purely time-dependent systematic error, spurious changes would be inferred for ϵ_{nn} and ϵ_{pp} but not ϵ_{np} . For two reasons, we do not think this type of error has a significant effect on the results (Fig. 1C). (i) Such an error would affect

the estimates of ϵ_{nn} and ϵ_{pp} equally, so the changes in dilatation would correspond to equal contributions from these strain components. This is clearly not entirely the case as ϵ_{nn} and ϵ_{pp} are not well correlated for the most part (Fig. 1C). (ii) An obvious source of systematic error in determining dilatation is the effect of not taking proper account of the atmospheric variables: temperature, pressure, and water vapor pressure. To test this possibility, we assumed that the observed dilatation is a linear function of these three variables and determined this function by a least-squares procedure; we found that none of the coefficients were statistically significant.

13. Currently there is substantial disagreement between strain changes inferred from the two-color Geodimeter data set and those recorded with a Sacks-Everson dilatometer at a depth of about 200 m within the northeast portion of the

Pearblossom network [M. J. S. Johnston, I. S. Sacks, A. T. Linde, D. Myren, *Eos* 63, 430 (1982)]. The fluctuations in dilatation recorded by the dilatometer are approximately an order of magnitude lower in amplitude than those inferred from the two-color Geodimeter data during corresponding time periods.

14. We thank M. L. MacKenzie, A. Rigoni, G. Oehler, J. Carson, R. Pilkington, D. Bates, and T. Von Tersch for participation in the field operations, A. Cole of the U.S. Forest Service at Pearblossom and W. Slawson of the University of British Columbia for support in initiating the program, and J. Blalock for permission to construct the Pearblossom observatory for the two-color Geodimeter. We acknowledge the contributions of J. C. Savage, W. H. Prescott, W. Thatcher, and M. Lisowski to this program.

24 March 1982; revised 12 October 1982

Crypts Are the Site of Intestinal Fluid and Electrolyte Secretion

Abstract. *The site of adenosine 3',5'-monophosphate-mediated fluid and electrolyte secretion across mammalian large intestine was found to be the crypts of Lieberkühn by means of two techniques. First, the formation of fluid droplets was visualized on the oil-covered mucosal surface directly over crypt duct openings when secretion was stimulated. Second, microelectrode impalement of individual surface and crypt cells revealed that only the crypt cells produced a pattern of secretagogue-induced alterations in membrane potential and resistance that was characteristic of secretory epithelia.*

The large intestine of mammals displays morphologic heterogeneity, consisting of two distinct structural regions: the surface epithelium and the crypts (1). The surface epithelium is composed primarily of columnar epithelial cells, whereas the epithelial cells and goblet cells (in a ratio of approximately 3 to 1) of the crypts surround a central duct that opens onto the mucosal surface. The intestine also shows functional heterogeneity. Colonic mucosa absorbs salt and water by way of an electrogenic Na^+ transport process that is stimulated by aldosterone (2) and inhibited by amiloride (3). In contrast, salt and water secretion results from the activity of an electrogenic Cl^- transport process that is stimulated by adenosine 3',5'-monophosphate (cyclic AMP) or agents that increase cellular cyclic AMP content (for example, theophylline, prostaglandin E_2 , cholera toxin, or vasoactive intestinal peptide) (4).

Studies of the electrophysiology of the surface cells of rabbit descending colon have disclosed the presence of electrogenic Na^+ absorption (5), but the site of electrogenic Cl^- secretion remains unresolved. Indirect evidence, derived primarily from studies of mammalian small intestine, suggests that the crypts are responsible for cyclic AMP-induced fluid and electrolyte secretion. This evidence includes the following. (i) Exposure of rabbit jejunum to hypertonic solutions damaged the villus cells and impaired glucose absorption but did not

alter the secretory response to cholera toxin (6). (ii) Exposure of rabbit jejunum to cycloheximide elicited morphologic changes in the crypt cells and inhibited secretion without affecting glucose absorption or the morphology of the villus cells (7). (iii) Brief exposure of rat or hamster jejunum to cholera toxin increased the concentration of cyclic AMP in villus cells and inhibited electrolyte absorption, whereas a prolonged exposure to the toxin was required to increase the cyclic AMP content of crypts and elicit electrolyte secretion (8). (iv) Gallbladder and flounder intestine display

electrolyte absorptive processes that are mechanically similar to those of mammalian small intestine, but these tissues contain no crypts and do not secrete in response to cyclic AMP (9).

In the present study, we used two direct techniques to identify the site of intestinal fluid and electrolyte secretion. We used rabbit descending colon *in vitro* as the experimental preparation because the absorptive and secretory processes have been well characterized and because the flat-surface epithelium and the crypts can be visualized separately. The tissue was stretched across a Lucite holding ring yielding an exposed tissue area of 1 cm^2 and mounted, mucosal surface up, on a microscope stage where it was examined with a Nikon phase-contrast microscope. The mucosal surface was dried and covered with oil while the serosal compartment was perfused with Ringer solution. As shown in Fig. 1A, the crypts and semitransparent surface epithelium can be readily distinguished.

Stimulation of secretion by addition of prostaglandin E_2 (PGE_2) to the serosal perfusate resulted in the appearance of small droplets of fluid on the mucosal surface (Fig. 1B). The droplets always appeared over the crypts. Fluid droplets could not be visualized over all crypts at all times. In many instances the secreted fluid spread over the surface epithelium rather than standing up in the oil as a readily visible bubble. Thus, bubbles that were initially visible because of the interface contrast between the oil and water phases would become invisible as fluid spread over the surface. This was especially true when secretion had pro-

Fig. 1. Light micrograph of colonic mucosa, *in vitro*, looking down on the mucosal surface. The serosal surface was continuously perfused with Ringer solution containing (in millimolar concentrations): Na, 143; K, 5.4; Ca, 1.2; Mg, 1.2; Cl, 123.7; HCO_3^- , 24; HPO_4^{2-} , 2.4; H_2PO_4^- , 0.6; and glucose, 10. This solution was aerated with 95 percent O_2 and 5 percent CO_2 and maintained at 37°C .

The mucosal surface was blotted gently with tissue paper and covered with a thin layer of water-equilibrated paraffin oil ($\times 175$). (A) Nonstimulated tissue. The crypts, (*d*, crypt duct openings) can be seen lying beneath the semitransparent surface epithelium. (B) Same area of tissue 10 minutes after the addition of PGE_2 ($10^{-6}M$) to the serosal bathing solution. Note location of fluid bubbles (*b*) over the crypt duct openings. The epithelium now appears slightly blurred because the fluid droplets have been brought into focus.

